NASA TECHNICAL NOTE

NASA TN D-6615

EFFECTS OF REYNOLDS NUMBER
AND BODY CORNER RADIUS ON
AERODYNAMIC CHARACTERISTICS OF
A SPACE SHUTTLE-TYPE VEHICLE
AT SUBSONIC MACH NUMBERS

by Leland H. Jorgensen and Jack J. Brownson

Ames Research Center
Moffett Field, Calif. 94035

NATIONAL AERONAUTICS AND SPACE ADMINISTRATION • WASHINGTON, D. C. • JANUARY 1972

0133211

1. Report No. NASA TN D-6615	2. Government Accession No.	3. Recipient's Catalog No.

4. Title and Subtitle EFFECTS OF REYNOLDS NUMBER AND BODY CORNER RADIUS ON AERODYNAMIC CHARACTERISTICS OF A SPACE SHUTTLE–TYPE VEHICLE AT SUBSONIC MACH NUMBERS	5. Report Date January 1972
	6. Performing Organization Code

7. Author(s) Leland H. Jorgensen and Jack J. Brownson	8. Performing Organization Report No. A-4153
	10. Work Unit No. 750-117-07-02-00-21

9. Performing Organization Name and Address NASA Ames Research Center Moffett Field, Calif., 94035	10. Work Unit No. 750-117-07-02-00-21
	11. Contract or Grant No.
	13. Type of Report and Period Covered Technical Note

12. Sponsoring Agency Name and Address NATIONAL AERONAUTICS AND SPACE ADMINISTRATION Washington, D. C. 20546	13. Type of Report and Period Covered Technical Note
	14. Sponsoring Agency Code

15. Supplementary Notes

16. Abstract

Static aerodynamic forces and moments were measured to study the effects of Reynolds number and body corner radius on the aerodynamic characteristics of a straight-wing space shuttle orbiter at subsonic speeds. A 0.02-scale model was tested at Mach numbers from 0.3 to 0.9 and Reynolds numbers from about 0.6×10^6 to 3×10^6, based on body width. The body alone and the body with its wing and horizontal tail attached were tested at angles of attack from 35° to 75°. The effects of rounding the body corners at the junctures connecting the bottom and sides were investigated for corner radii from 0 to 8.5 percent of the body width.

At low subsonic Mach numbers ($M_\infty \simeq 0.3$) the aerodynamic characteristics are affected significantly by changes in Reynolds number and body corner radius. With increase in Mach number to $M_\infty = 0.9$ the effect of Reynolds number seems to vanish, but a significant effect of body corner radius remains.

17. Key Words (Suggested by Author(s)) Shuttle vehicle Body corner radius Viscous crossflow Reynolds number effects	18. Distribution Statement Unclassified — Unlimited

19. Security Classif. (of this report) Unclassified	20. Security Classif. (of this page) Unclassified	21. No. of Pages 33	22. Price* $3.00

SYMBOLS

A   planform area of body with zero corner radius

b   body width

b_0 reference body width (fig. 1(d))

C_{d_n} crossflow drag coefficient, $\dfrac{C_N}{\sin^2 \alpha}$

C_m pitching-moment coefficient, $\dfrac{\text{pitching moment}}{q_\infty A b_0}$

C_N normal-force coefficient, $\dfrac{\text{normal force}}{q_\infty A}$

C_n body axis yawing-moment coefficient, $\dfrac{\text{yawing moment}}{q_\infty A(2s)}$

h   body height

M_∞ free-stream Mach number

M_n crossflow Mach number

q_∞ free-stream dynamic pressure

Re   Reynolds number based on reference body width b_0

Re_n crossflow Reynolds number, $Re \sin \alpha$

r   body corner radius (fig. 1(d))

s   wing semispan

V_n component of free-stream velocity normal to body axis

x   axial distance from body nose

x_{ac} axial distance from body nose to aerodynamic force center

α angle of attack

β angle of sideslip of the model vertical reference plane

Λ angle between sting axis and body axis

EFFECTS OF REYNOLDS NUMBER AND BODY CORNER RADIUS ON

AERODYNAMIC CHARACTERISTICS OF A SPACE SHUTTLE–TYPE

VEHICLE AT SUBSONIC MACH NUMBERS

Leland H. Jorgensen and Jack J. Brownson

Ames Research Center

SUMMARY

To aid in assessing effects of Reynolds number and body corner radius on the aerodynamic characteristics of a straight-wing space shuttle orbiter at subsonic speeds, static aerodynamic forces and moments have been measured for a 0.02-scale model at Mach numbers from 0.3 to 0.9 and Reynolds numbers from about 0.6×10^6 to 3×10^6, based on body width. For angles of attack from $35°$ to $75°$, normal-force and pitching-moment coefficients were measured for the body alone as well as for the body with wing and tail attached. With the model at $60°$ angle of attack, yawing-moment coefficients were measured for sideslip angles from $-4°$ to $+8°$. To determine effects of rounding the body corners at the junctures connecting the sides to the bottom, tests were made with corner radii varying from 0 to 8.5 percent of the body width.

Results show that at low subsonic Mach numbers ($M_\infty = 0.3$) the high angle-of-attack normal-force and aerodynamic-force-center characteristics of the body alone and the body with its wing and horizontal tail attached are affected significantly by changes in Reynolds number and body corner rounding. With increase in Mach number up to $M_\infty = 0.9$ the effect of Reynolds number seems to vanish, and the effect of corner rounding diminishes but still remains significant. The dependence of the pitch characteristics on Reynolds number diminishes as Mach number is increased to 0.6 and is practically eliminated at $M_\infty = 0.9$.

It has been found that there is close similarity, in both magnitude and change with Reynolds number, between the crossflow drag coefficients for the shuttle body at high angles of attack and two-dimensional square cylinders at $90°$ angle of attack. From this similarity it is concluded that most of the shuttle test data for $M_\infty = 0.3$ lie within the critical Reynolds number range, the range in which the crossflow drag coefficient decreases from high to low values as the Reynolds number increases from subcritical to critical. At this low Mach number the highest test Reynolds number, which was about one-fourth the expected flight value, was not sufficiently above the critical value to assure accurate determination of high angle-of-attack flight aerodynamics. It appears, however, that data nearly representative of that for flight Reynolds numbers can be obtained at lower Reynolds numbers in wind-tunnel tests at Mach numbers above about 0.7, provided proper attention is paid to close matching of body corner rounding on wind-tunnel models and flight vehicles.

INTRODUCTION

An exploratory investigation has been conducted to determine the effects of Reynolds number and body corner radius on the static aerodynamic characteristics of a space shuttle-type orbiter vehicle at subsonic speeds. This vehicle, originally proposed by the NASA Manned Spacecraft Center (ref. 1), has a large flat-bottomed body with a straight wing and tail. The corners at the junctures connecting the bottom to the sides of the body are rounded to alleviate corner heating when the vehicle enters and descends through the atmosphere at a constant angle of attack of about 60°. This high angle attitude is to be maintained by aerodynamic means until the vehicle decelerates to a Mach number of less than 0.5 at an altitude of about 40,000 feet.

In this investigation, tests of a 0.02-scale model were made in three wind tunnels at the Ames Research Center for Mach numbers from 0.3 to 0.9 and Reynolds numbers from about 0.6×10^6 to 3×10^6, based on body width. Six-component static aerodynamic force and moment coefficients were measured for angles of attack from about 35° to 75°. With the model at an angle of attack of 60°, aerodynamic coefficients also were obtained for sideslip angles from about -4° to +8°. Data have been obtained for the body alone as well as for the body with its wing and horizontal tail attached. To determine effects of body corner rounding, tests were made with sharp body corners as well as with rounded corners having radii up to 8.5 percent of the body width. Basic data from the tests are presented in references 2, 3, and 4.

A study of the basic data revealed significant effects of Reynolds number and body corner radius on the aerodynamic normal-force and pitching-moment coefficients for subsonic Mach numbers. The purpose of this report is to present and discuss selected data that illustrate these effects.

APPARATUS AND TESTS

Model

Sketches of the test model are shown in figure 1, and photographs in figure 2. The model is a 0.02-scale version of an early space shuttle orbiter originally proposed by the NASA Manned Spacecraft Center (ref. 1). It was constructed so that the body alone could be tested as well as the body with the wing and horizontal tail attached. Body corner radii of 0, 4.0, 6.3, and 8.5 percent of the reference body width were investigated (fig. 1(d)). The body was sting mounted on a six-component internal strain gage balance alined with the body axis. The sting supporting the balance and body entered the rearward top of the body (fig. 2(b)) at an angle of either 36° or 55° to the body axis (fig. 1(a)).

Measurements, Test Conditions, and Wind Tunnels

For both the body alone and the body with the wing and tail attached, six-component aerodynamic force and moment data were obtained for angles of attack from about 35° to 75°. With the body-wing-tail model at 60° angle of attack, data also were obtained for sideslip angles

from about -4° to +8°. All of the data obtained in this investigation are presented in references 2, 3, and 4. Results selected for analysis in this report were obtained at the conditions specified in table 1.

TABLE 1.– TEST CONDITIONS AND WIND TUNNELS

Figure	Model	r/b_O	M_∞	$Re \times 10^{-6}$	α, deg	β, deg	Wind tunnel
3,4	Body alone	0,0.040,	0.3	0.63 to 2.93	60	0	12-foot
		0.063,0.085	.6	.83 to 2.33			11- by 11-foot
		0,0.063, 0.085	.9	.83 to 2.50			
5	Body alone	0.063	.3	.63 to 2.50	35 to 75	0	12-foot
			.6	.83 to 2.33	40 to 70		11- by 11-foot
			.9	.83 to 2.50			
9	Body-wing-tail	0.085	.3	.65 to 2.50	60	0	12-foot
			.6				
			.7	.84 to 2.34			11- by 11-foot
			.8				
			.9	.83 to 2.49			
12,13,14	Body-wing-tail	0	.3	0.57	45 to 73	0	6- by 6-foot
		0.085	.3	.65,2.49	35 to 75		12-foot
			.6	.84,2.34	40 to 70		11- by 11-foot
			.9	.83,2.49			
15	Body-wing-tail	0	.3	.56	60	- 4 to 8	6- by 6-foot
			.6	1.09			
			.9	.81			
		0.085	.3	.84,2.46			12-foot
			.6	.63,1.91		- 4 to 6	11- by 11-foot
			.9				

To obtain the specified Mach and Reynolds numbers, the tests were conducted at Ames Research Center in three wind tunnels: the 12-Foot Pressure Wind Tunnel, the 11- by 11-Foot Transonic Wind Tunnel, and the 6- by 6-Foot Wind Tunnel.

In table 2 the maximum test Reynolds numbers for the body-wing-tail model are compared with the estimated full-scale flight values, assuming the model is 0.02 scale. The test Reynolds numbers vary from about one-fourth of the flight value at $M_\infty = 0.3$ to about one-half at $M_\infty = 0.9$. For a booster vehicle somewhat similar to the orbiter investigated here, the flight Reynolds numbers would be more than two or three times those given in table 2.

TABLE 2.– COMPARISONS OF MAXIMUM TEST REYNOLDS NUMBERS WITH ESTIMATED FLIGHT REYNOLDS NUMBERS

M_∞	Maximum test $Re \times 10^{-6}$	Estimated flight $Re \times 10^{-6}$	$\dfrac{\text{Test Re}}{\text{Flight Re}}$
0.3	2.50	10	0.25
.6	2.34	7	.33
.9	2.49	5	.50

RESULTS AND DISCUSSION

This discussion concerns data that show significant effects of Reynolds number and body corner radius on the aerodynamic characteristics of the body alone and the body with the wing and horizontal tail attached. The discussion is divided into two major parts, body alone and body-wing-tail.

Body Alone

Figure 3 shows the effect of Re on C_N for the body alone with various r at 60° angle of attack and at $M_\infty = 0.3$, 0.6, and 0.9. At $M_\infty = 0.3$ (fig. 3(a)) there is a large effect of Re on C_N as r is increased from zero ($r/b_0 = 0$) to 8.5 percent of the body width ($r/b_0 = 0.085$). Except for the body with sharp corners ($r/b_0 = 0$), there is a "bucket effect" in C_N as Re increases; that is, C_N decreases rather abruptly to a minimum value and then increases as Re continually increases. Unfortunately, the test Reynolds numbers do not extend high enough from the bucket bottom for a reasonable determination of C_N to be made at the expected flight Reynolds number of about 10×10^6. This bucket effect appears to increase with increasing r, but fortunately the effect also decreases with increasing Mach number. At $M_\infty = 0.6$ (fig. 3(b)) it is barely discernible, and at $M_\infty = 0.9$ (fig. 3(c)) it has disappeared.

A somewhat similar effect of Reynolds number on the aerodynamic normal force center (x_{ac}/b_0) is shown in figure 4. Here the aerodynamic force center, measured from the body nose (in body widths), is also affected the greatest by Reynolds number changes at $M_\infty = 0.3$.

In addition to the large effect of Reynolds number on C_N and x_{ac}/b_0, the data in figures 3 and 4 show a large effect of small changes in body corner rounding. Throughout the Reynolds number range C_N decreases significantly with increase in r/b_0 from 0 to 8.5 percent (fig. 3). The aerodynamic force center generally moves forward with increase in r/b_0 (fig. 4), although this is not always the case at the lowest Mach number, $M_\infty = 0.3$ (see fig. 4(a)). The effect of corner rounding on C_N and x_{ac}/b_0 is the largest at the lowest Mach number but still persists up to the highest Mach number, $M_\infty = 0.9$, where the Reynolds number effect has essentially disappeared.

Although the Reynolds number bucket effect is shown in figures 3 and 4 for the body at only $\alpha = 60°$, it was found to exist throughout the entire high angle-of-attack range investigated ($35° \leqslant \alpha \leqslant 75°$). In figure 5, for example, a large effect of Re on the variation of C_N with α is shown for the body with edge radii 6.3 percent of the body width. As in figure 3, it is seen that C_N is greatly affected by Re only at the lowest Mach number, $M_\infty = 0.3$. (Compare figs. 5(a), (b), and (c).)

The Reynolds number effect (figs. 3 through 5) might have been expected because of a similar effect documented (refs. 5 and 6) for the crossflow drag of two-dimensional square cylinders with rounded corners. In figure 6 data from references 5 and 6 are plotted showing the effect of Re_n on C_{d_n} for two-dimensional square cylinders with corner radii from $r/b_0 = 0.021$ to 0.333. All data are for a M_n well below the critical value of about 0.4. Also included in figure 6 are data from the present investigation for the body tested at $\alpha = 60°$ and $M_\infty = 0.3$ ($M_n = 0.26$). With the assumption

that the flow normal to the body axis may be considered independent of the axial flow, C_N data from figure 3(a) were converted to C_{d_n} data by the relation, $C_{d_n} = C_N/\sin^2 \alpha$. Reynolds numbers were converted to crossflow values by $Re_n = Re \sin \alpha$.

Figure 6 shows close similarity between the variation of C_{d_n} with Re_n for two-dimensional square cylinders and the body being investigated at $\alpha = 60°$. Most of the data appear to lie within the critical Reynolds number range, or the range in which the drag coefficients decrease from high values (laminar flow) to low values (turbulent flow). All results indicate a rather large effect of corner radius on both C_{d_n} and critical Re_n. As corner radius increases, values of both C_{d_n} and critical Re_n appear to decrease.

There is a significant effect of r on C_{d_n} at all Reynolds numbers shown in figure 6. The effect of corner radius on C_{d_n} is further demonstrated in figure 7 by a plot of C_{d_n} versus r/b_0 for a subcritical Reynolds number of $Re_n \approx 10^5$. Experimental values of C_{d_n} decrease significantly with small increase in r relative to b_0. The initial rate of decrease in C_{d_n} with increase in $K = r/b_0$ is much greater than the linear decrease predicted by Newtonian theory (fig. 7).

All the results in figures 6 and 7 only serve to amplify the important question, "What are the C_{d_n} levels along the body at crossflow Reynolds numbers near the expected full-scale flight value?" At the expected flight crossflow Reynolds number of about 9×10^6, the C_{d_n} levels for square cross sections with rounded corners are unknown, and there is appreciable scatter in the known data for circular cross sections. In figure 8 the scatter in the available data for circular cross sections can be observed. This figure (taken from ref. 8) summarizes the present state of knowledge in the variation of C_{d_n} with Re_n for Re_n from 10^5 to 10^7. References 8, 9, and 10 contain detailed discussions of these data.

If shuttle vehicles of the type studied in this investigation are to fly at high angles of attack and at low subsonic Mach numbers, data should be obtained at higher Reynolds numbers.

Body-Wing-Tail

Figure 9 shows the effects of Mach number and Reynolds number on C_N and aerodynamic force center x_{ac}/b_0 for the body-wing-tail model with the body corners rounded ($r/b_0 = 0.085$) and the body at $\alpha = 60°$. As expected, C_N increases with increase in Mach number over the Reynolds number range. For all of the Mach numbers from 0.3 to 0.9, the C_N results decrease somewhat with increase in Reynolds number, but, as for the body alone (fig. 3(a)), the greatest decrease occurs at $M_\infty = 0.3$. There appears to be little effect of Reynolds number on x_{ac}/b_0 except at $M_\infty = 0.3$; here there is a significant rearward shift with increasing Reynolds number.

In figure 10 the effect of Reynolds number on C_N and x_{ac}/b_0 for the body-wing-tail model is compared with that for the body alone with $r/b_0 = 0.085$, $\alpha = 60°$, and $M_\infty = 0.3$. In general C_N decreases considerably with increase in Re for both the body alone and the body with wing and tail, and the body contribution to C_N for the body-wing-tail varies from about 50 percent at the lowest Reynolds numbers to about 30 percent at the highest (fig. 10(a)). The aerodynamic force center for the body alone moves forward with increase in Reynolds number from about 0.6×10^6 to 1.3×10^6, then generally reverses and moves rearward with further increase in Reynolds number. Because of

lack of data for the body-wing-tail model, the variation of x_{ac}/b_0 with Re is not as clearly defined; however, the overall movement is rearward over the Re range investigated.

In figure 11 the effect of Mach number on C_N for the body-wing-tail model is compared with that for the body alone with $r/b_0 = 0.085$ and $\alpha = 60°$. Results are shown for both a low and a high test Reynolds number (0.8×10^6 and 2.5×10^6). As expected, for both the body-wing-tail and the body alone configurations, C_N increases with increase in Mach number, and the body contribution to C_N for the body-wing-tail is significant at all Mach numbers. At $M_\infty = 0.3$ the body develops about 40 percent of the body-wing-tail normal force at the low Reynolds number and about 30 percent at the high Reynolds number. At Mach numbers of 0.6 and above, the body develops about 60 percent of the body-wing-tail normal force at both Reynolds numbers.

As for the body alone, the Reynolds number effect on C_N and x_{ac}/b_0 extends over most of the high angle-of-attack range investigated and is the largest at $M_\infty = 0.3$. Also, there is a large effect of body corner radius at this low Mach number. Both of these effects are shown in figures 12 and 13. At $M_\infty = 0.3$ (fig. 12(a)), C_N decreases significantly with both increase in r/b_0 and increase in Re. As M_∞ increases, the effect of Reynolds number decreases considerably (see figs. 12(b) and (c)). Based on the results for the body alone, it is believed that the effect of body corner radius on the aerodynamics of the model with wing and tail also decreases as M_∞ increases. This effect, however, was not investigated in tests of the body-wing-tail model.

Figure 14 shows the effects of r and Reynolds number on the variation of C_m with angle of attack. At $M_\infty = 0.3$ (fig. 14(a)) and at the highest Reynolds number (2.49×10^6), it is encouraging to find that the model with $r/b_0 = 0.085$ shows a stable variation of C_m with α over the entire high α range investigated. At a much lower Reynolds number (0.65×10^6) the curve for the same r/b_0 indicates a positive peak in pitching moment for angles of attack from about 50 to 60°. This undesirable effect appears to increase as the r is decreased. As M_∞ increases from 0.3 to 0.9 the positive peak in pitching moment at the lower Reynolds number persists and, in fact, is present at both high and low Reynolds numbers at $M_\infty = 0.9$. (Compare figs. 14(a), (b), and (c).)

Because the model was not tested with a vertical tail, the measured yawing-moment coefficients might not be too significant. However, they show large effects of Reynolds number and corner radius and are presented for reference in figure 15.

CONCLUDING REMARKS

At low subsonic Mach numbers ($M_\infty \simeq 0.3$) the high angle-of-attack normal-force and aerodynamic-force-center characteristics of the body alone and the body with its wing and horizontal tail attached are affected significantly by changes in Reynolds number and amount of corner rounding at the juncture of the body sides and bottom. With increase in Mach number up to $M_\infty = 0.9$ the effect of corner rounding diminishes but still remains significant. The dependence of the pitch characteristics on Reynolds number diminishes as M_∞ is increased to 0.6 and is practically eliminated at $M_\infty = 0.9$. Sideslip results are also sensitive to changes in Reynolds number and corner rounding at all Mach numbers investigated.
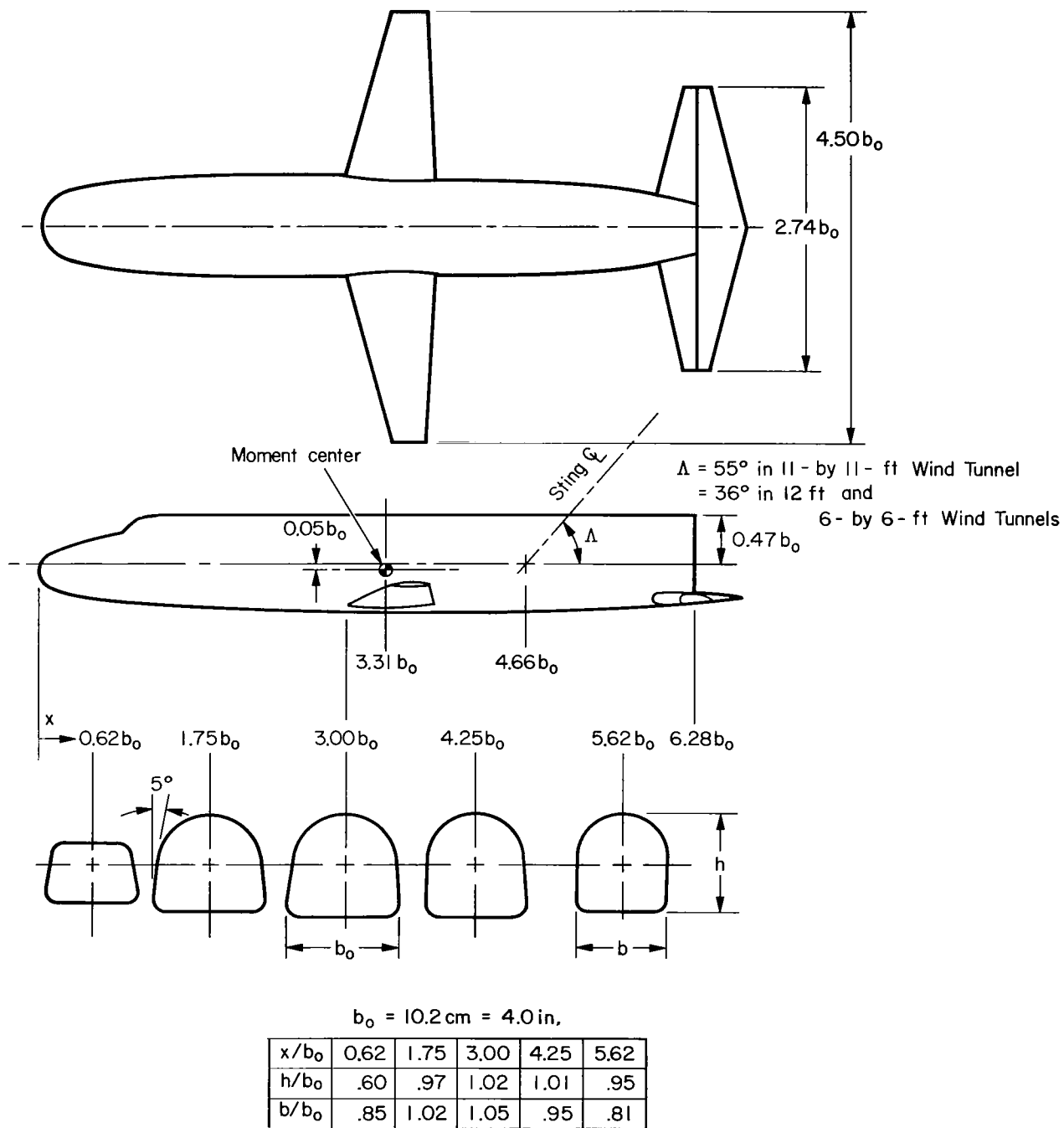
There is close similarity, in both magnitude and change with Reynolds number, between the crossflow drag coefficients for the shuttle body at high angles of attack and two-dimensional square cylinders at 90° angle of attack. From this similarity it is concluded that most of the test data for this particular shuttle configuration at $M_\infty = 0.3$ lie within the critical Reynolds number range, the range in which the crossflow drag coefficient decreases from high to low values as the Reynolds number increases from subcritical to critical. At this low Mach number the highest test Reynolds number, which was about one-fourth the estimated flight value, was not sufficiently above the critical value to assure accurate determination of high angle-of-attack flight aerodynamics. It appears, however, that data nearly representative of that for flight Reynolds numbers can be obtained at lower Reynolds numbers in wind-tunnel tests at Mach numbers above about 0.7, provided proper attention is paid to close matching of body corner rounding on wind-tunnel models and flight vehicles.

The results of this investigation suggest that, if shuttle vehicles are to be flown back into the atmosphere at very high angles of attack to low subsonic Mach numbers, further effort should be made to obtain wind-tunnel data at higher Reynolds numbers.

Ames Research Center
    National Aeronautics and Space Administration
        Moffett Field, California, 94035, Sept. 24, 1971

REFERENCES

1. Faget, Max: Space Shuttle: A New Configuration. J. Astronaut. & Aeron., vol. 8, no. 1, Jan. 1970, pp. 52-61.

2. Brownson, Jack J.; Graham, Ralph E.; Olson, Deloy; and Cambell, Jack: Static Stability Characteristics of the Manned Spacecraft Center Straight-Wing Space Shuttle Orbiter: Preliminary Tests (M = 0.25–2.0). NASA TM X–62,053, 1971.

3. Brownson, Jack J.; Graham, Ralph E.; and Banducci, David: Static Stability Characteristics of Manned Spacecraft Center Straight-Wing Space Shuttle Orbiter: Effect of Reynolds Number and Body Corner Radius at M ⩽ 0.5. NASA TM X–62,054, 1971.

4. Brownson, Jack J.; and Whitnah, A. M.: Static Stability Characteristics of a Manned Spacecraft Center Straight-Wing Space Shuttle Orbiter: Effect of Reynolds Number and Body Corner Radius (M = 0.6–1.35). NASA TM X–62,056, 1971.

5. Delany, Noel K.; and Sorensen, Norman E.: Low-Speed Drag of Cylinders of Various Shapes. NASA TN 3038, 1953.

6. Polhamus, Edward C.: Effect of Flow Incidence and Reynolds Number on Low-Speed Aerodynamic Characteristics of Several Noncircular Cylinders With Applications to Directional Stability and Spinning. NASA TR R–29, 1059.

7. Hoerner, Sighard F.: Fluid-Dynamic Drag. Published by the author, 148 Busteed Dr., Midland Park, New Jersey, 1965.

8. Jones, George W., Jr.; Cincotta, Joseph J.; and Walker, Robert W.: Aerodynamic Forces on a Stationary and Oscillating Circular Cylinder at High Reynolds Numbers. NASA TR R–300, 1969.

9. Roshko, Anatol: Experiments on the Flow Past a Circular Cylinder at Very High Reynolds Number. J. Fluid Mech., vol. 10, pt. 3, May 1961, pp. 345–356.

10. Schmidt, Louis V.: Fluctuating Force Measurements Upon a Circular Cylinder at Reynolds Numbers up to 5×10^6. NASA TM X–57,779, 1966.

4.50b_0

2.74b_0

Moment center

0.05b_0

Sting C_L

Λ = 55° in 11- by 11- ft Wind Tunnel
= 36° in 12 ft and
6- by 6- ft Wind Tunnels

Λ

0.47b_0

3.31b_0 4.66b_0

x

0.62b_0 1.75b_0 3.00b_0 4.25b_0 5.62b_0 6.28b_0

5°

h

b_0 b

b_0 = 10.2 cm = 4.0 in.

x/b_0	0.62	1.75	3.00	4.25	5.62
h/b_0	.60	.97	1.02	1.01	.95
b/b_0	.85	1.02	1.05	.95	.81

(a) Plan and elevation views of body-wing-tail model

Figure 1.- Model geometry.

(b) Half of wing

(c) Half of horizontal stabilizer
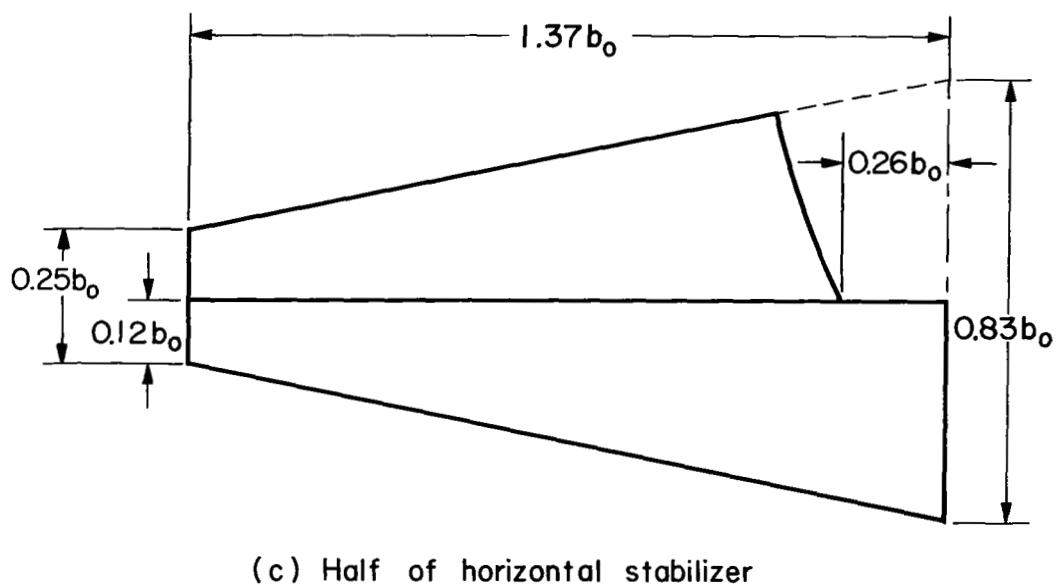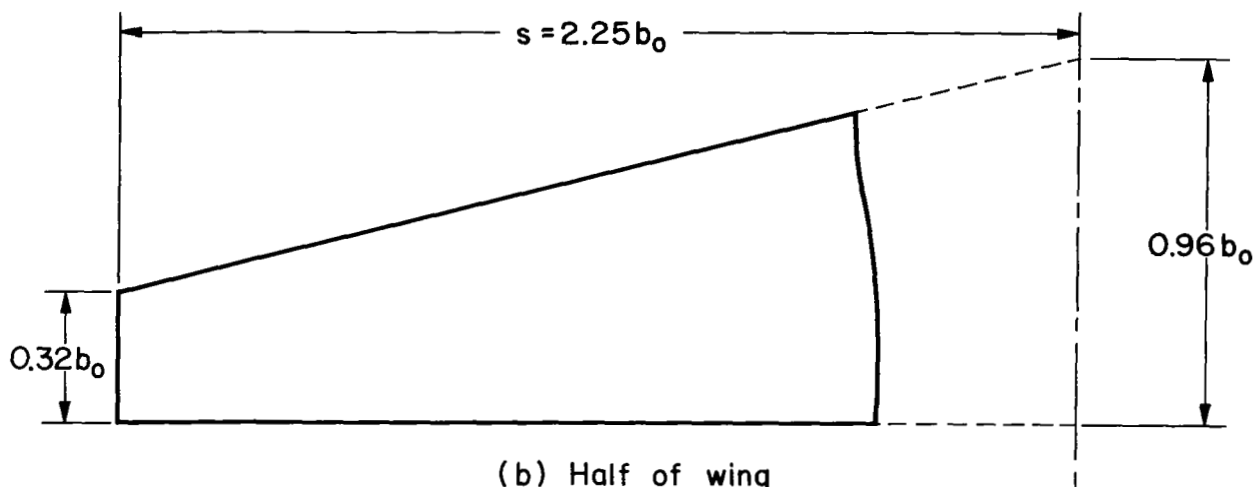
Note: Airfoil sections for both wing and stabilizer
    are NACA 0014-64 at root (body $\math{C}_L$) and NACA 0010-64
    at tip.

Figure 1.- Continued.
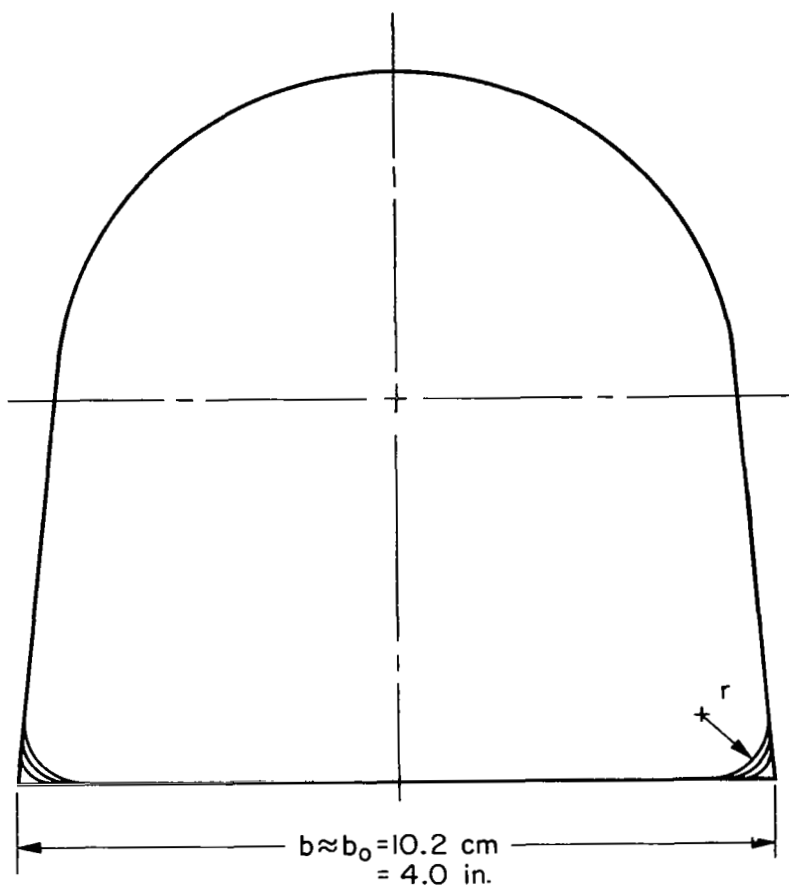
r, cm	$\dfrac{r}{b_0}$
0	0
0.41	0.040
.64	.063
.86	.085

$b \approx b_0 = 10.2$ cm = 4.0 in.

(d) Body reference cross section (at $x = 3b_0$)
with various corner radii

Figure 1.- Concluded.

11
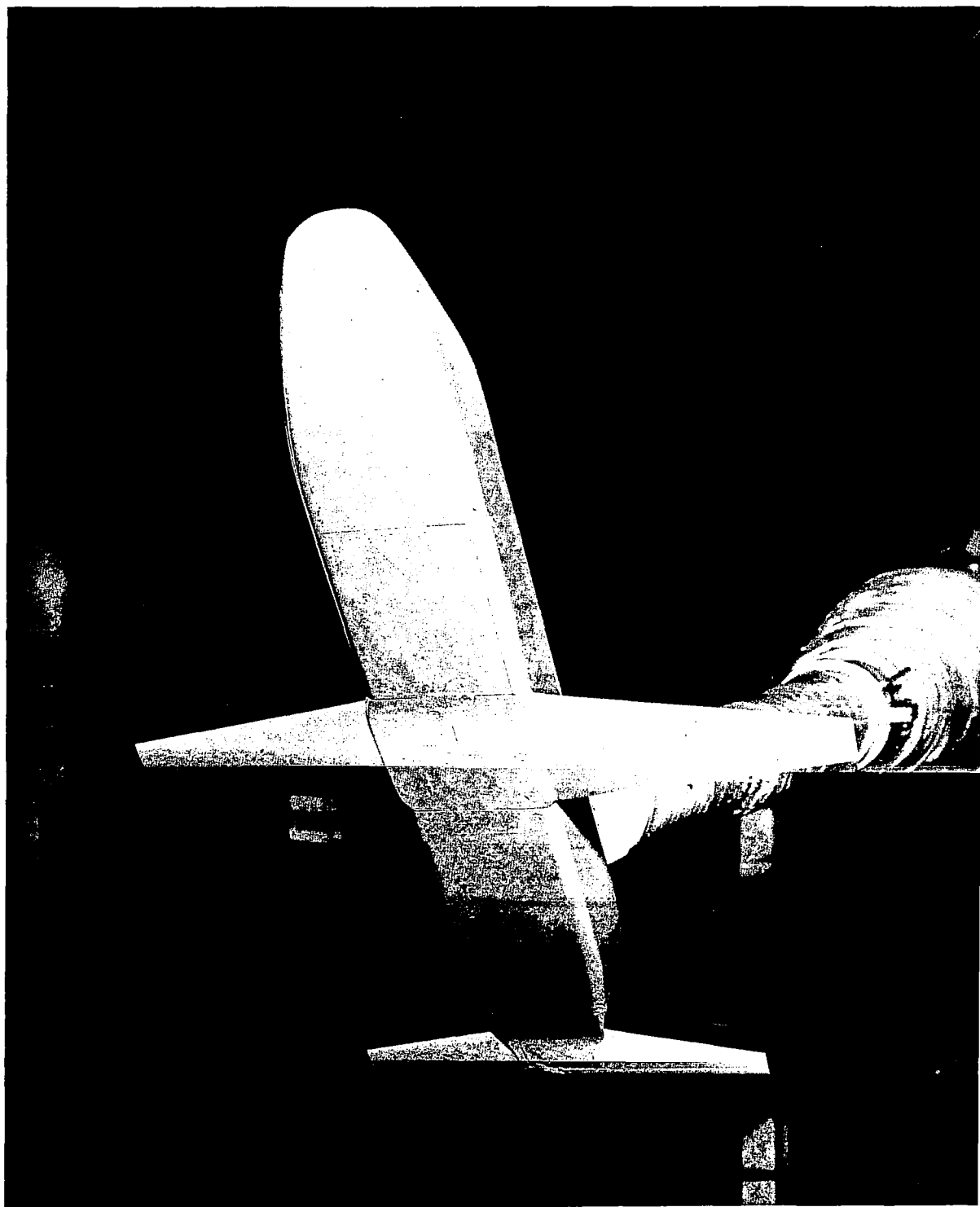
(a) Bottom view.

Figure 2.- Photographs of body-wing-tail model.
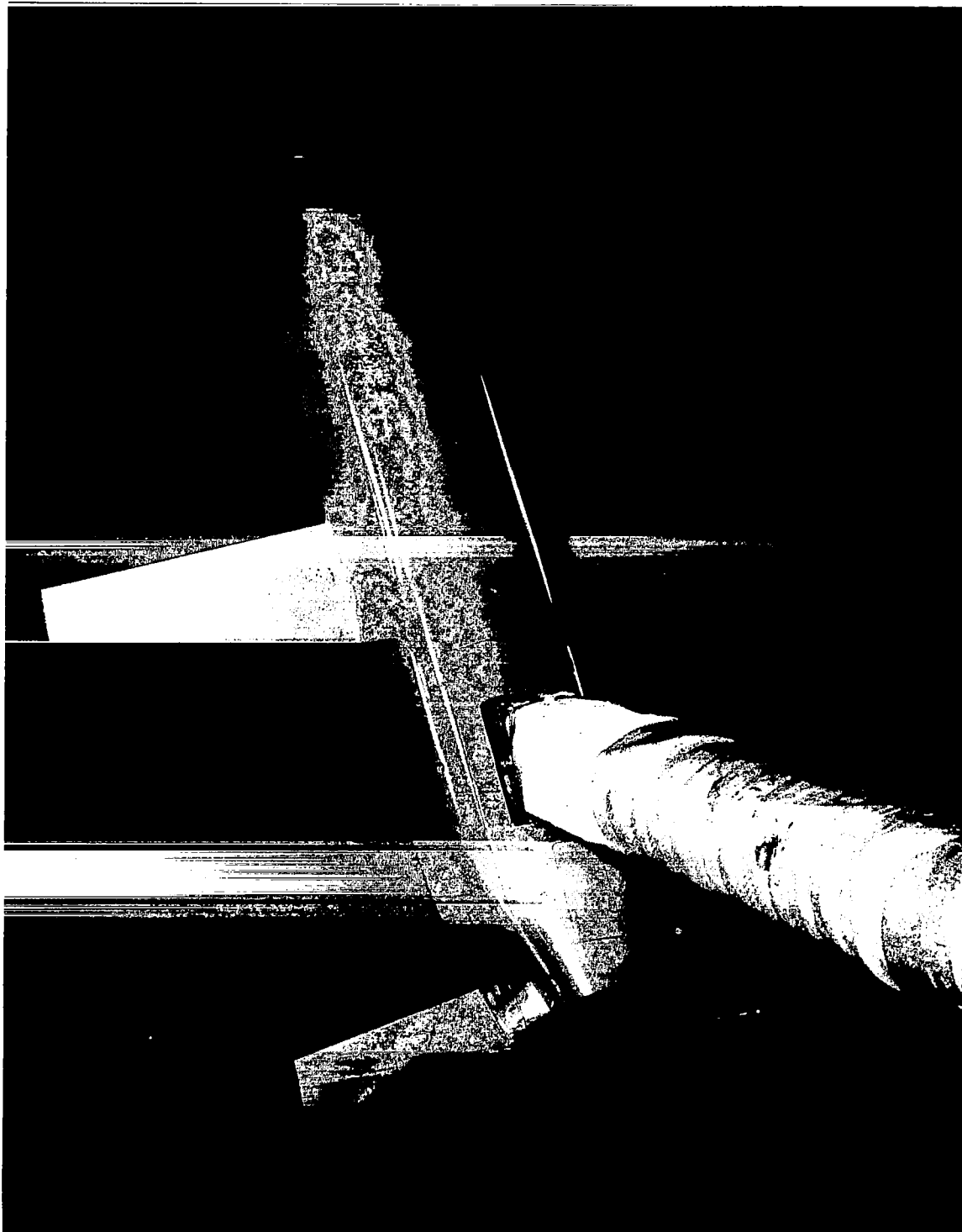
(b) Top view.

Figure 2.- Concluded.
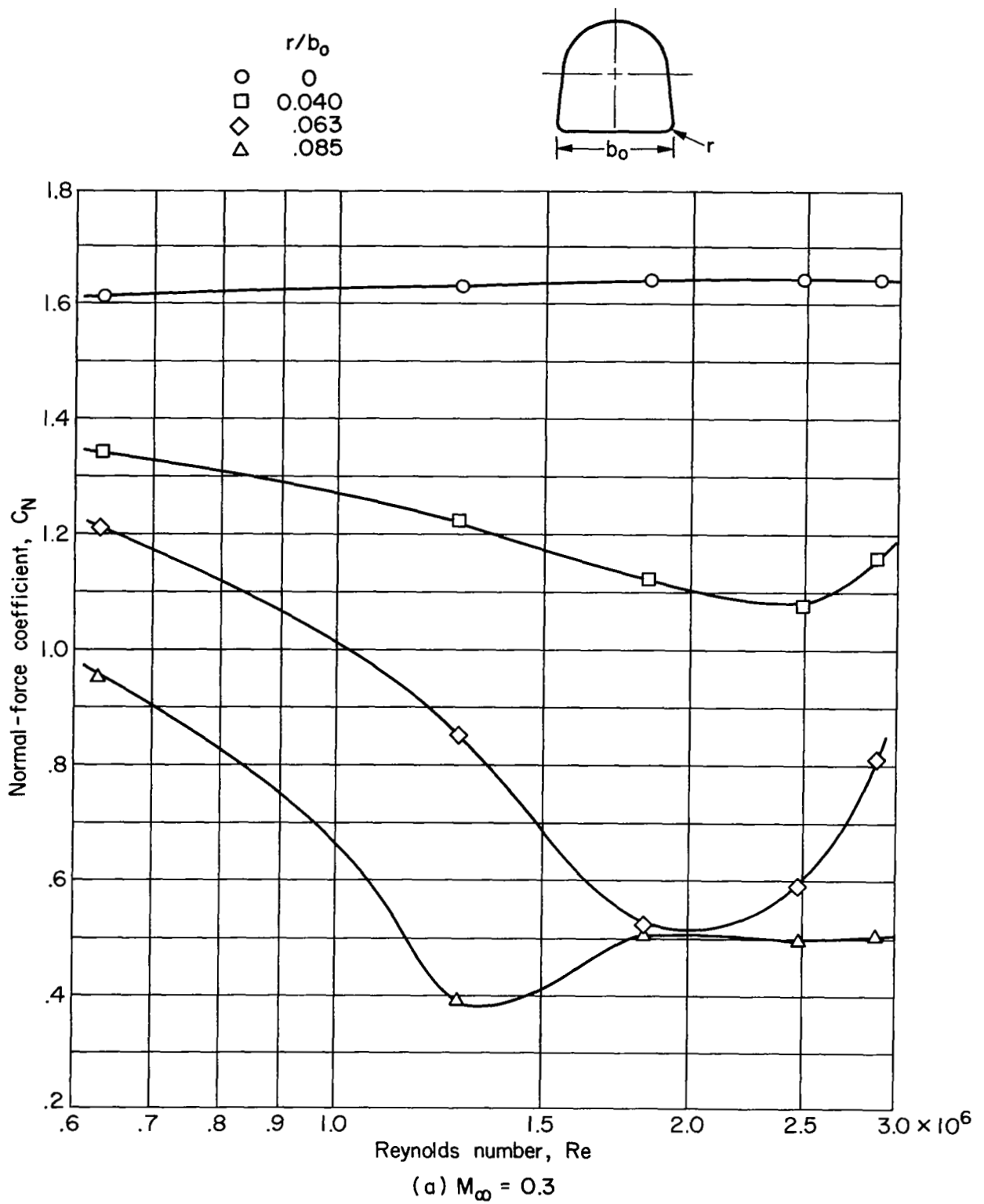
Figure 3.- Effect of Reynolds number on normal-force coefficient for body alone with various corner radii at $\alpha = 60°$.

14
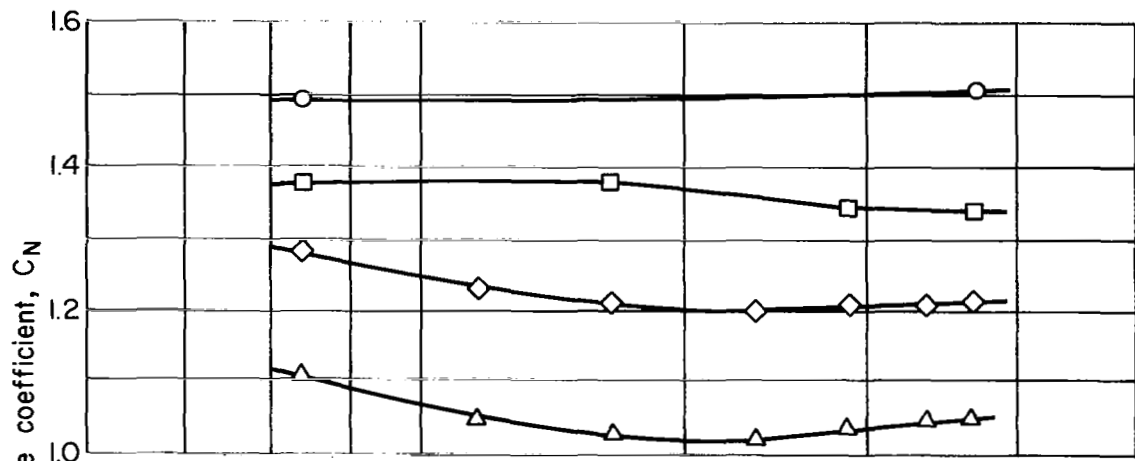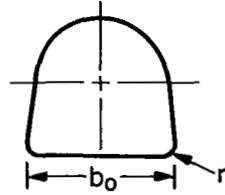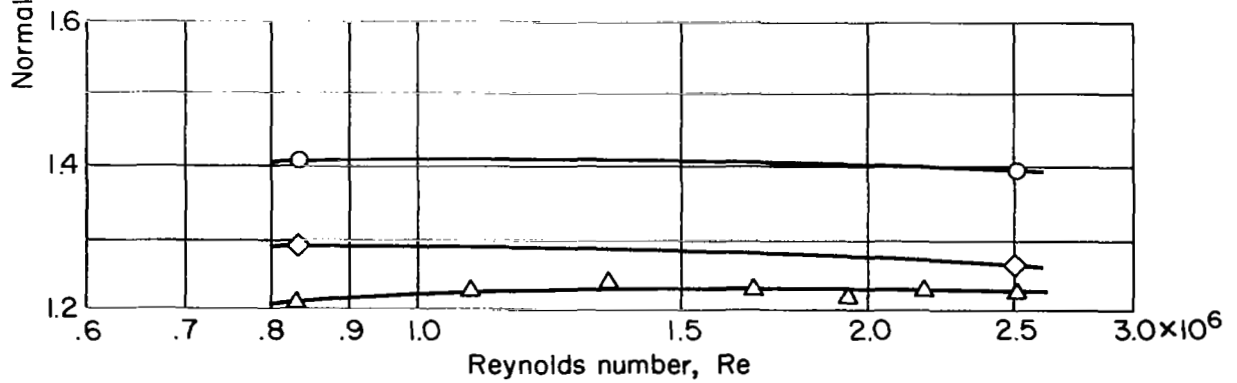
Figure 3.- Concluded.
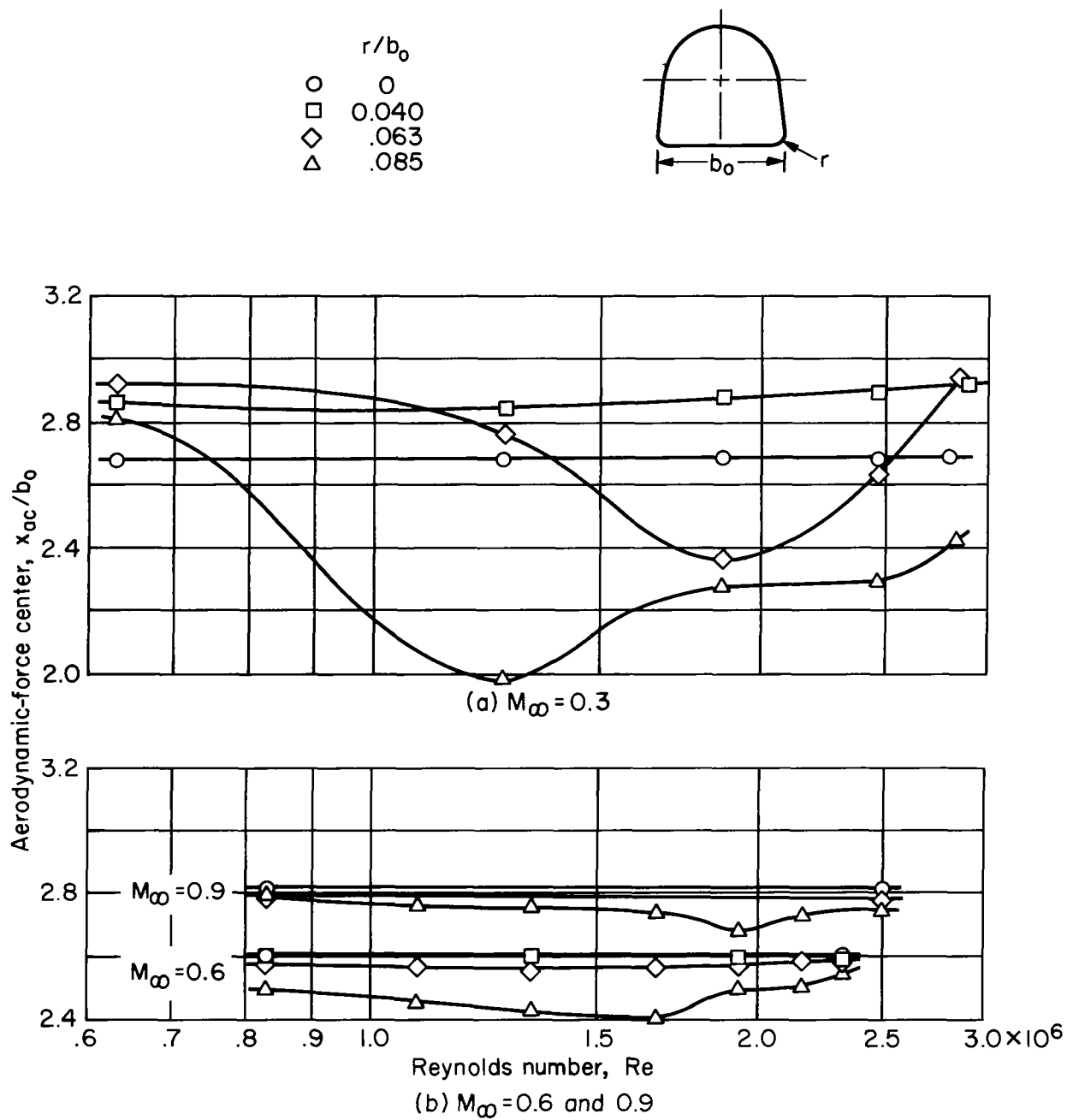
Figure 4.- Effect of Reynolds number on aerodynamic force center for body alone with various corner radii at $\alpha = 60°$.
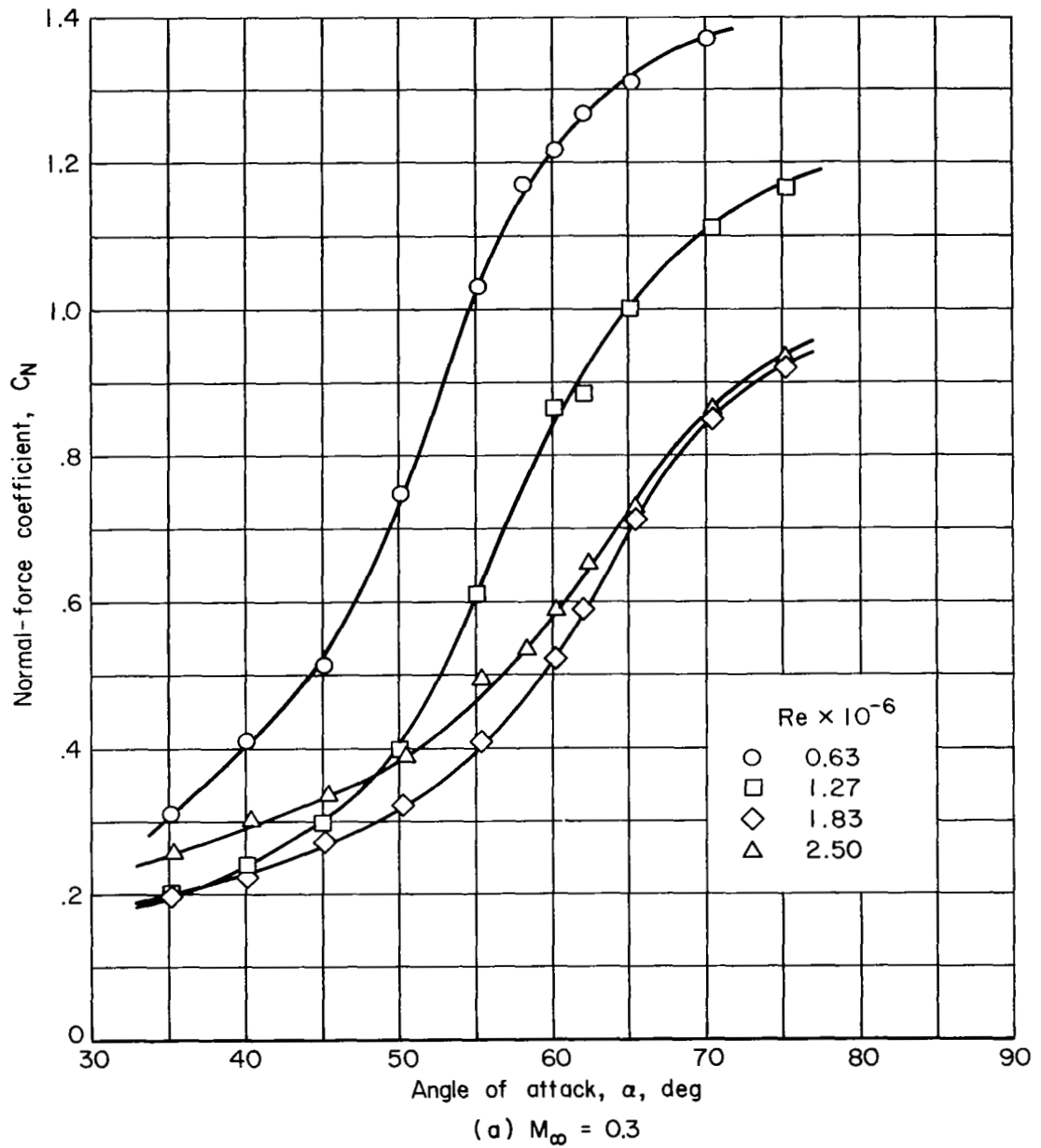
Figure 5.- Effect of Reynolds number on variation of normal-force coefficient with angle of attack for body alone with rounded corners ($r/b_O = 0.063$).

(b) $M_\infty = 0.6$

(c) $M_\infty = 0.9$
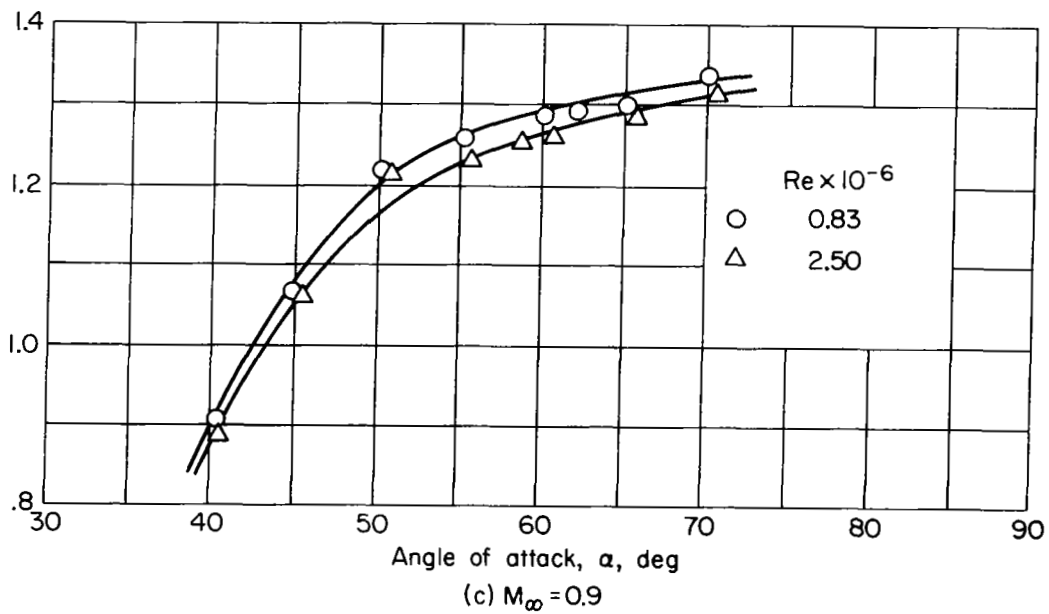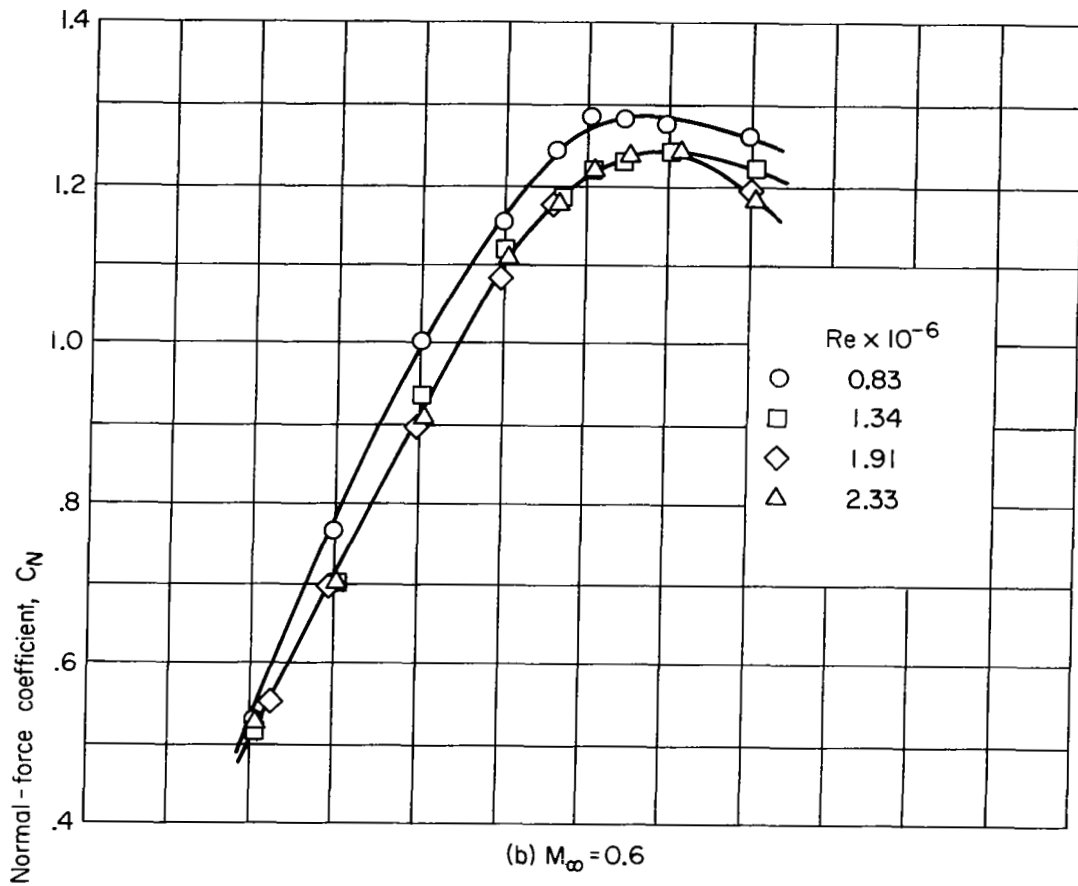
Figure 5.- Concluded.
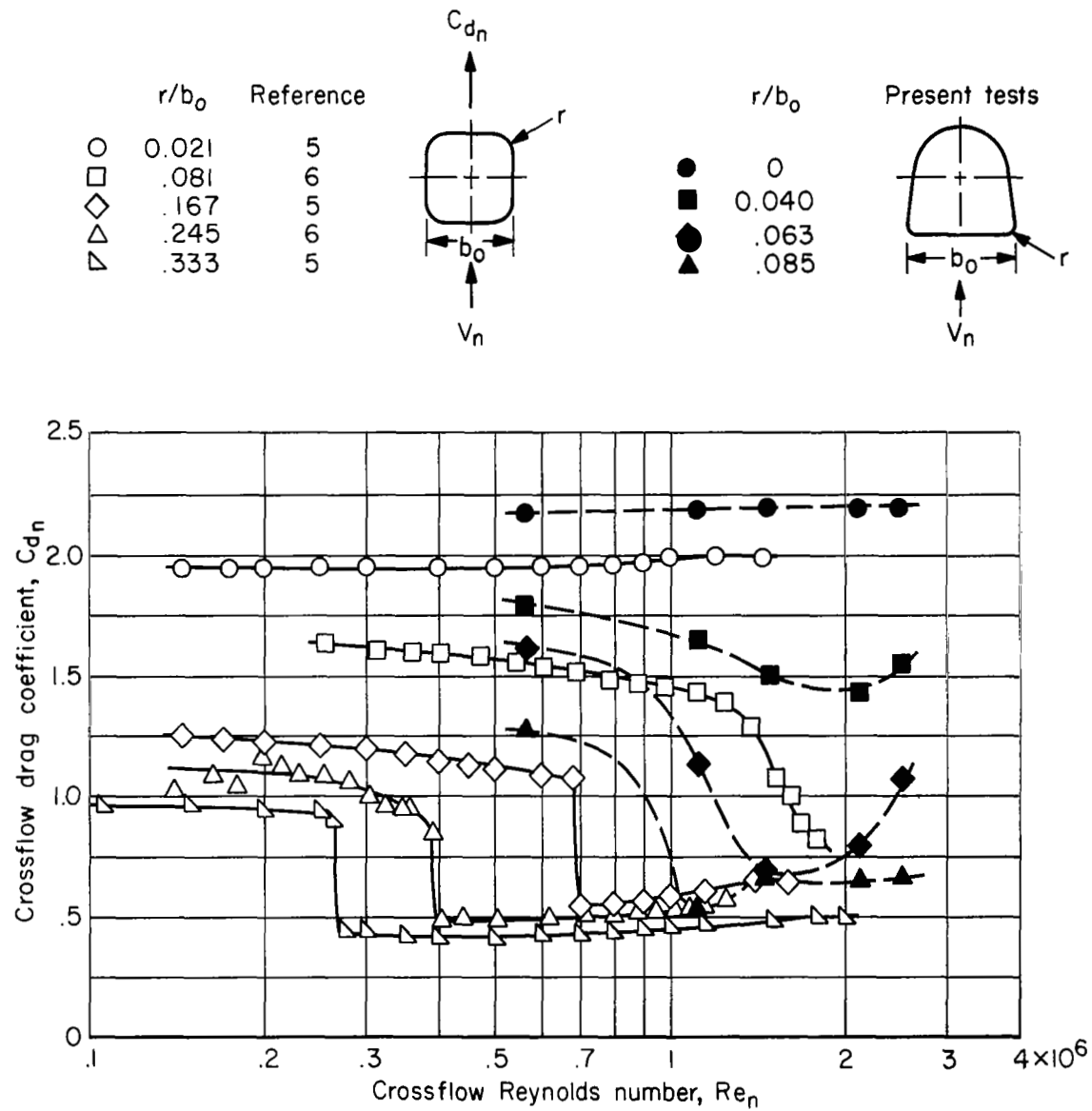
Figure 6.- Effect of crossflow Reynolds number on crossflow drag coefficient for two-dimensional square cylinders and for body alone with various corner radii (tested at $\alpha = 60°$); $M_n < 0.3$.
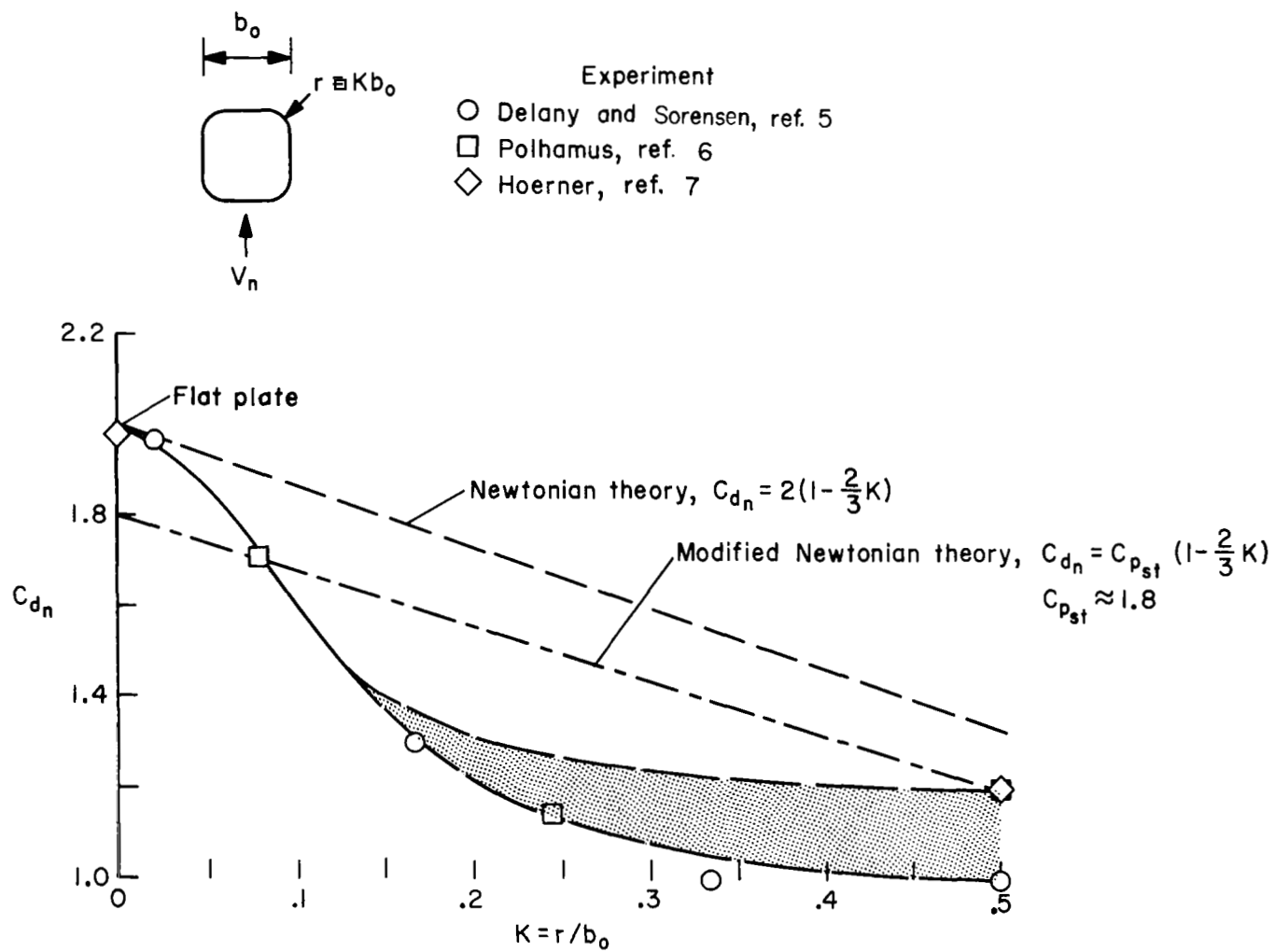
Figure 7.- Effect of corner radius on crossflow drag coefficient of two-dimensional square cylinders in incompressible flow; $Re_n \approx 10^5$.
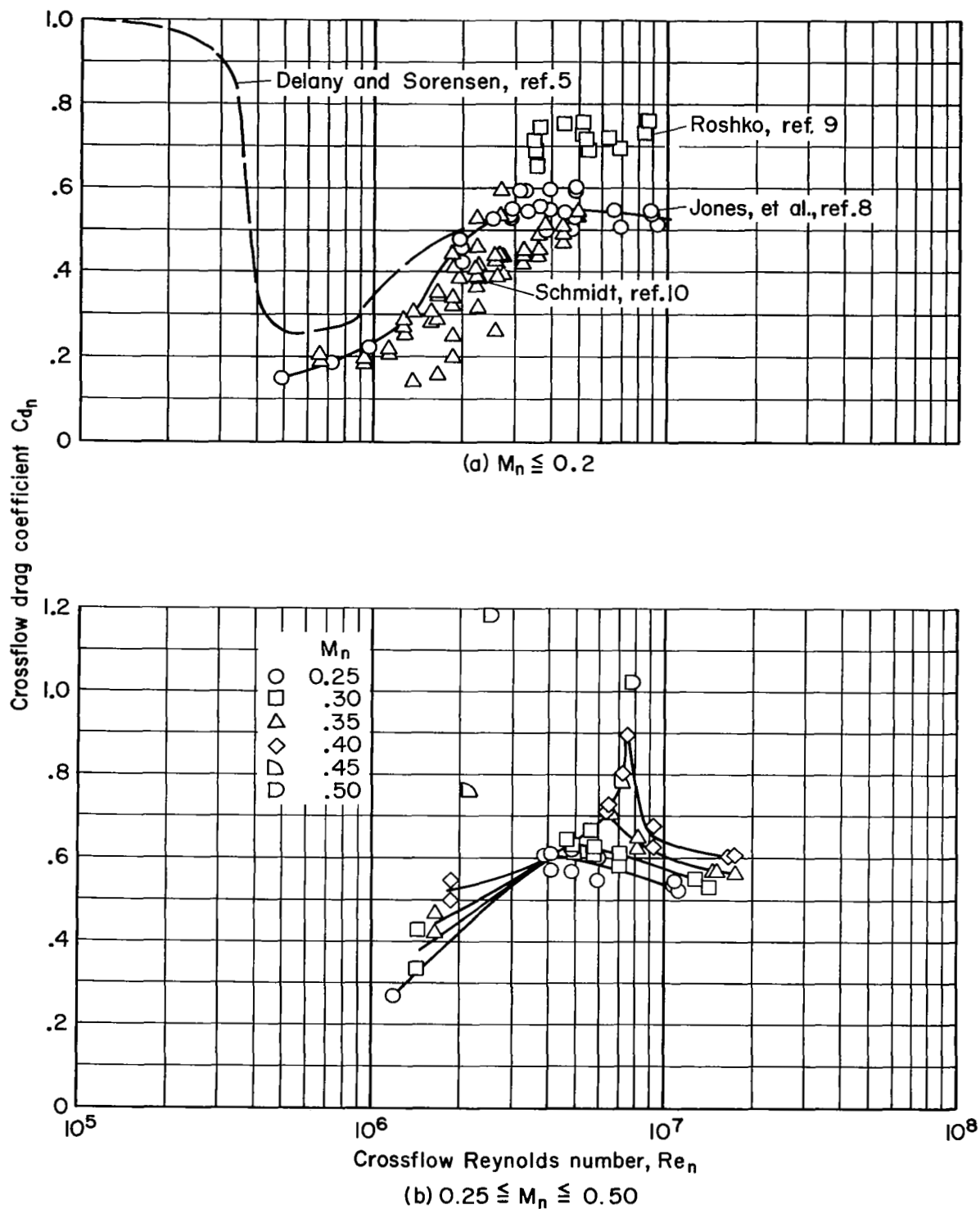
Figure 8.- Variation of crossflow drag coefficient with crossflow Reynolds number for circular cylinders at supercritical Reynolds numbers (from ref. 8).

(a) C_N vs. Re

(b) x_{ac}/b_0 vs. Re

Figure 9.- Effects of Mach number and Reynolds number on aerodynamic characteristics of body-wing-tail model at various Mach numbers; $\alpha = 60°$ and body $r/b_0 = 0.085$.
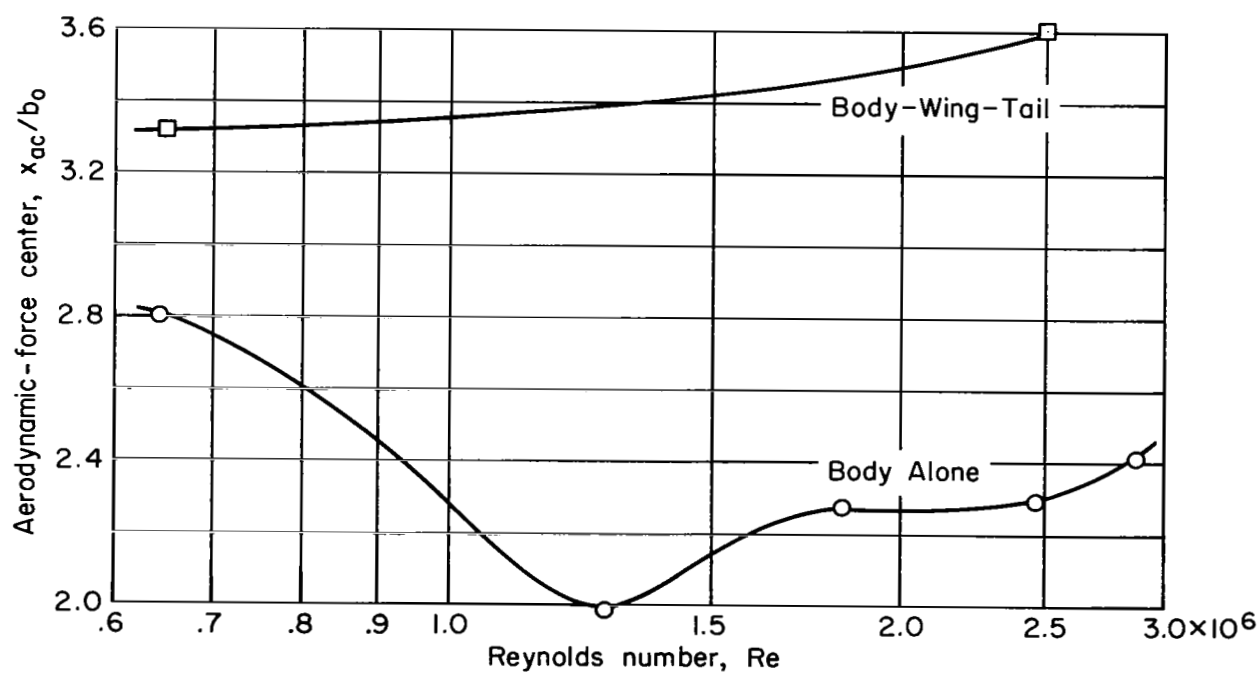
Figure l0.- Effect of Reynolds number on comparison of body-wing-tail with body alone aerodynamic characteristics for $r/b_0 = 0.085$; $\alpha = 60°$, and $M_\infty = 0.3$.
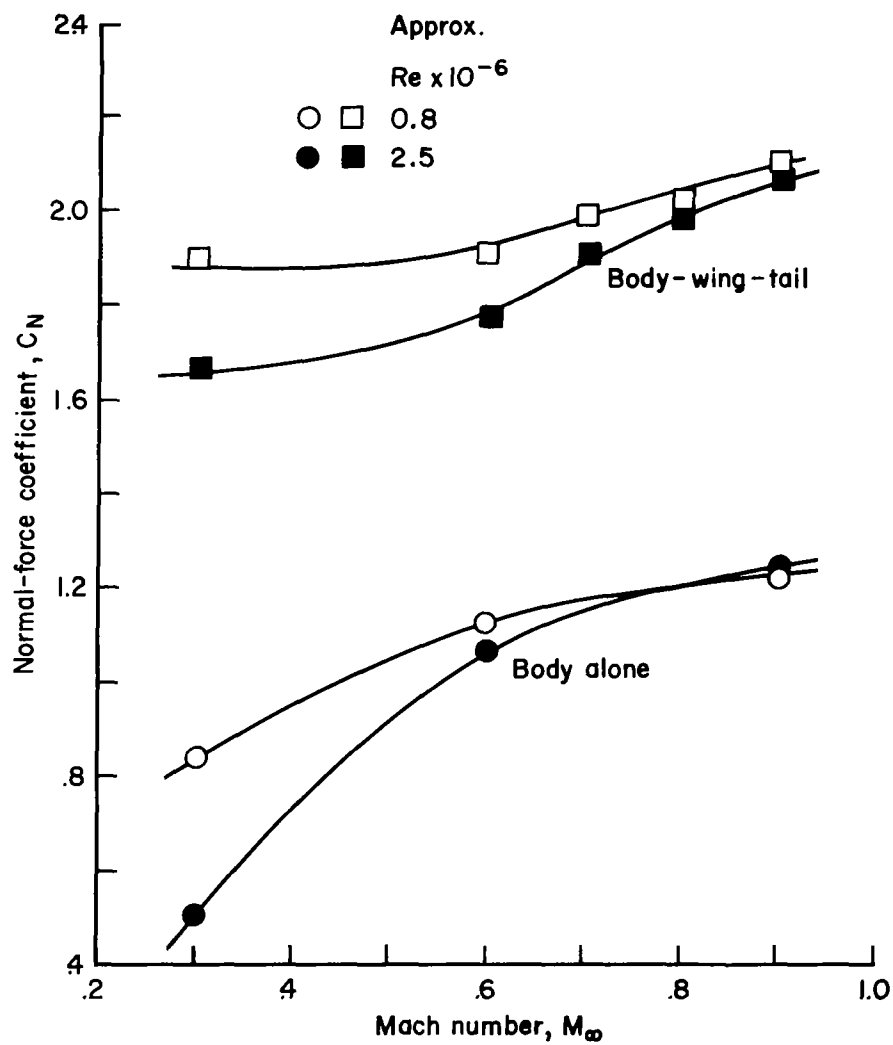
Figure 11.- Effect of Mach number on comparison of body-wing-tail with body alone normal-force coefficients for $r/b_0 = 0.085$ and $\alpha = 60°$.
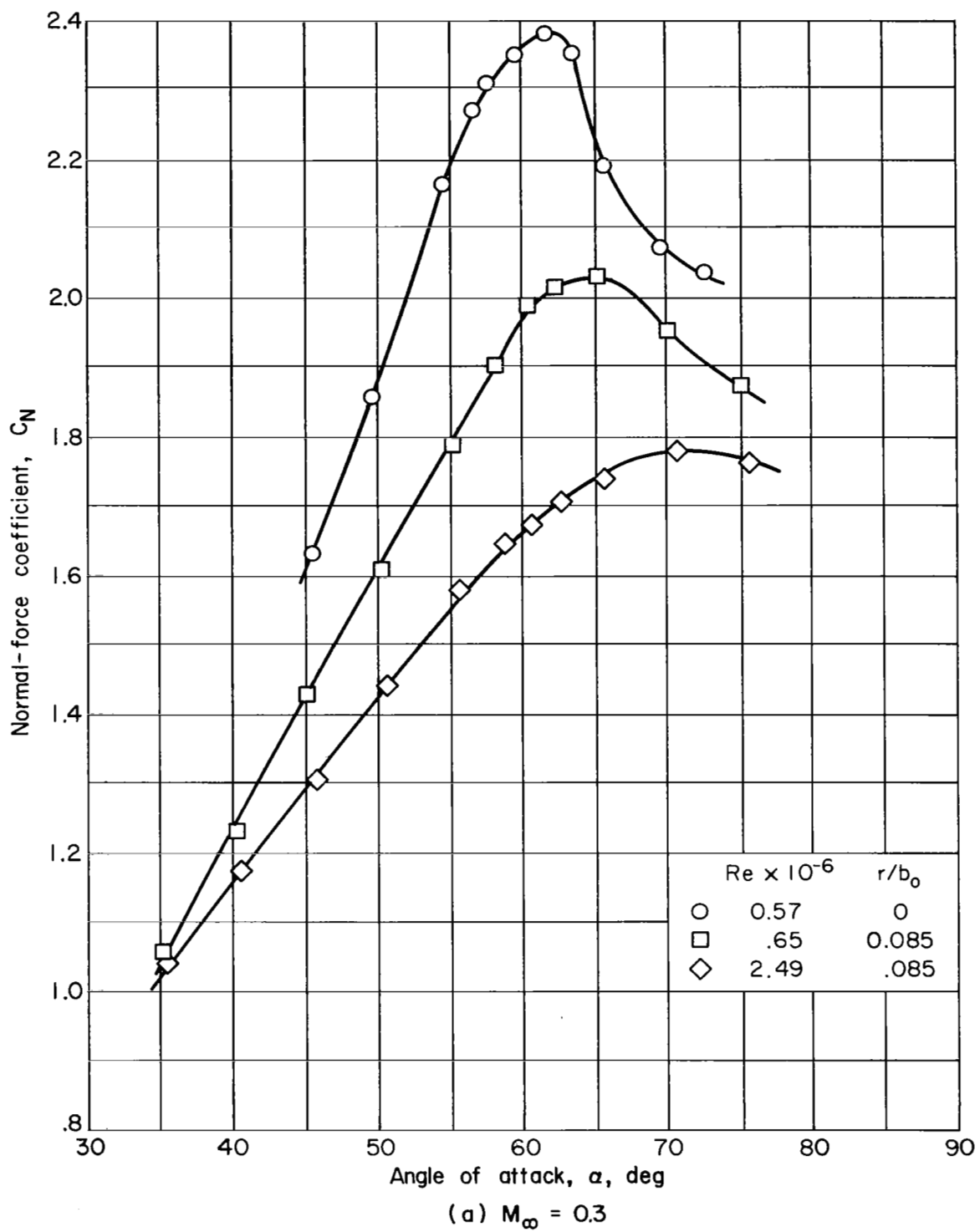
Figure 12.- Effects of body corner radius and Reynolds number on variation of normal-force coefficient with angle of attack for body-wing-tail model.
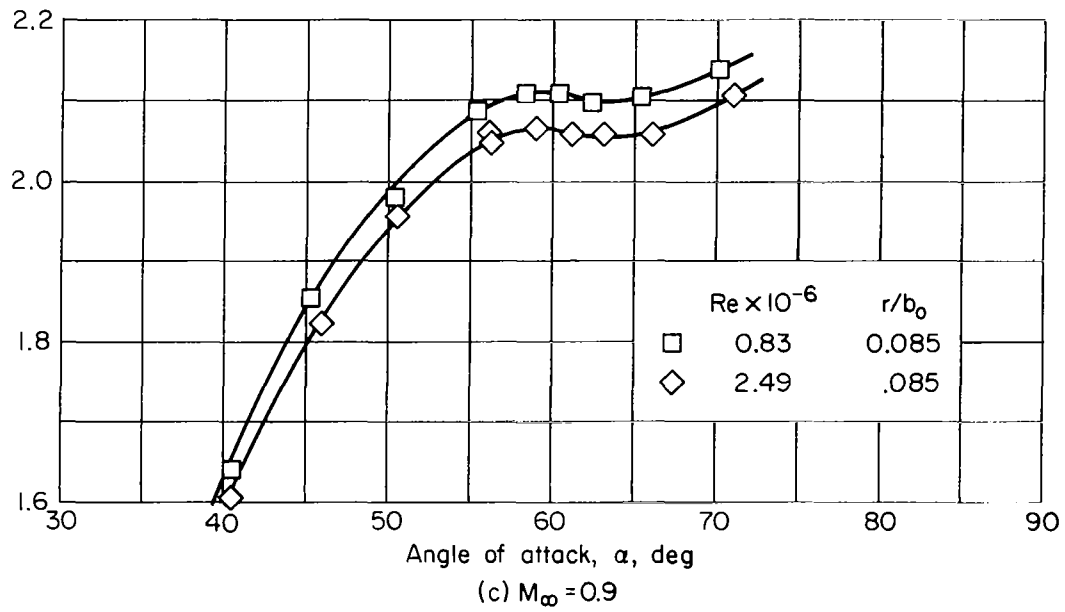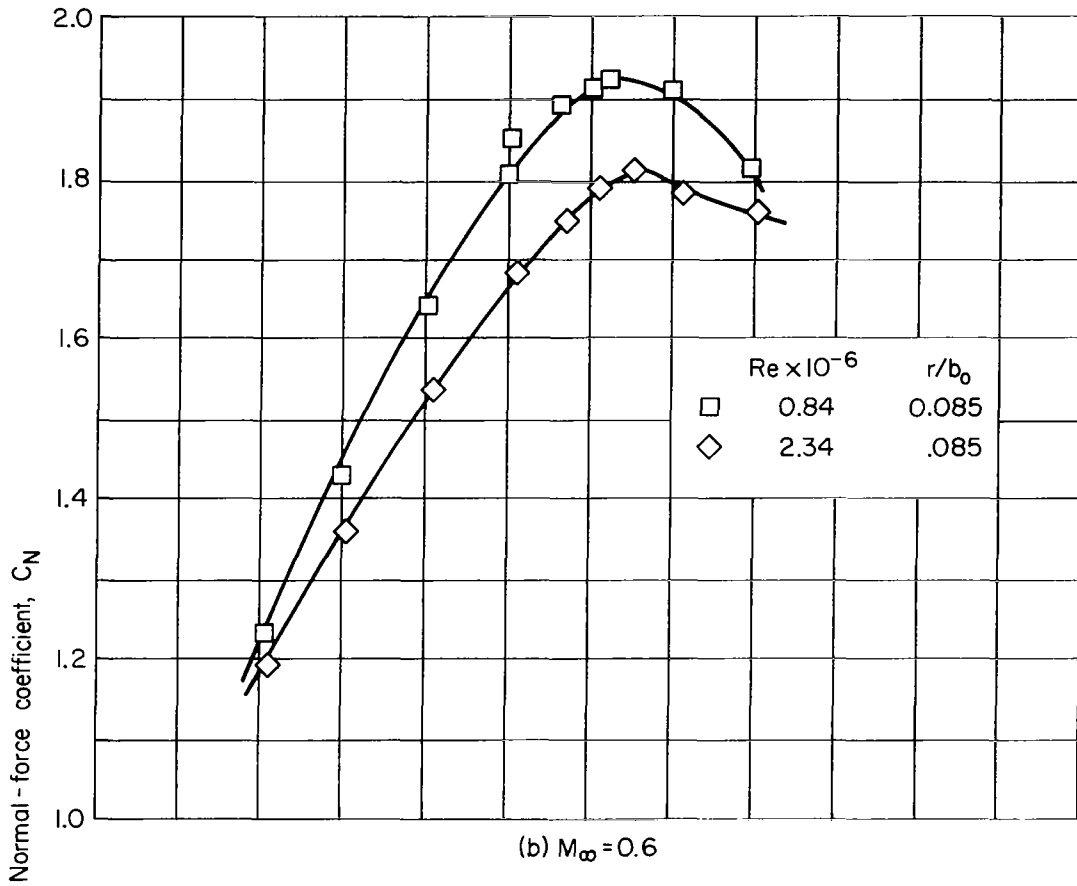
Normal - force coefficient, C_N
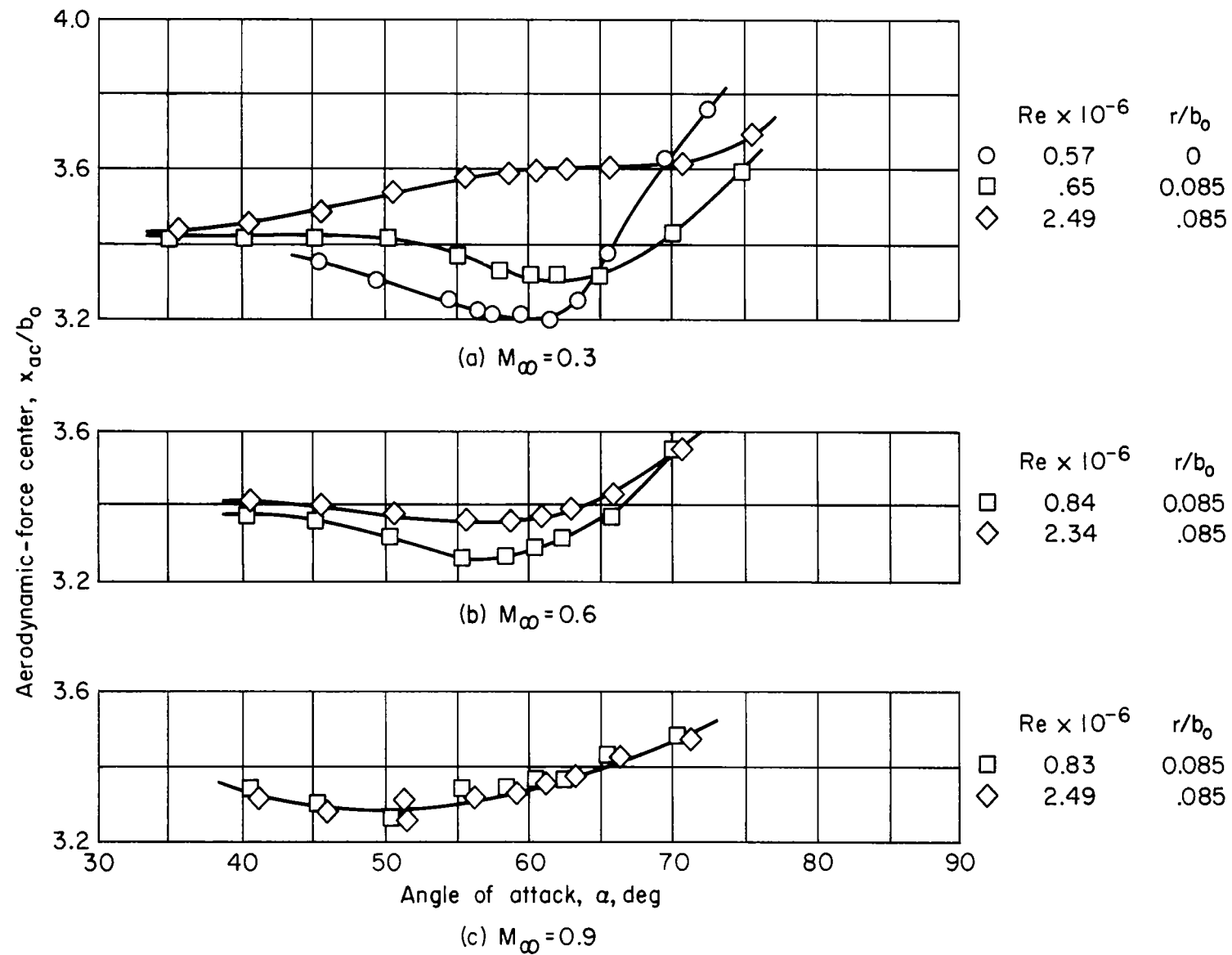
2.0

1.8

1.6

1.4

1.2

1.0

	Re $\times 10^{-6}$	r/b_0
□	0.84	0.085
◇	2.34	.085

(b) $M_\infty = 0.6$

2.2

2.0

1.8

1.6

	Re $\times 10^{-6}$	r/b_0
□	0.83	0.085
◇	2.49	.085

30   40   50   60   70   80   90

Angle of attack, α, deg

(c) $M_\infty = 0.9$

Figure 12.- Concluded.

Figure 13.- Effects of body corner radius and Reynolds number on variation of aerodynamic force center with angle of attack for body-wing-tail model.
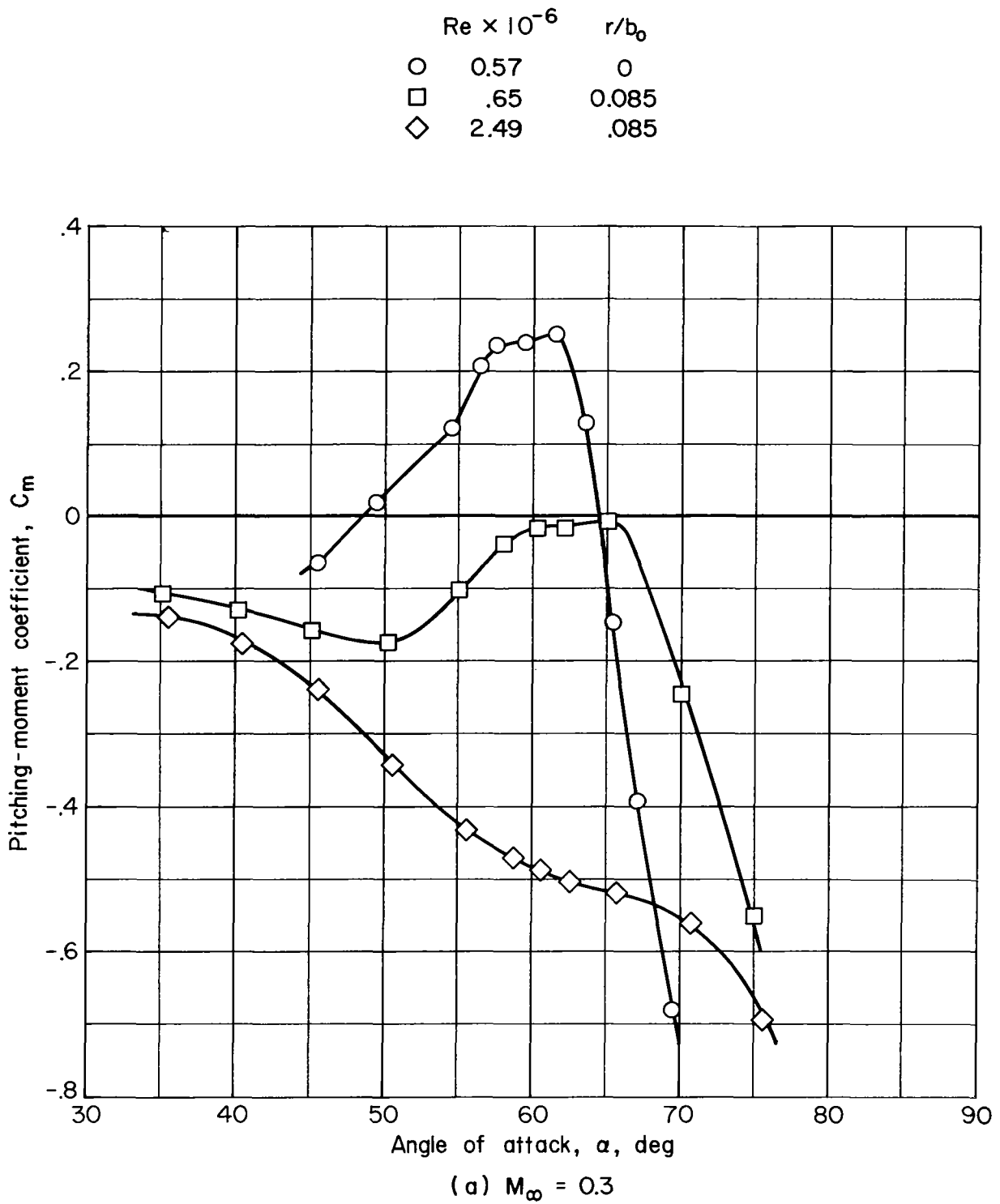
Figure 14.- Effects of body corner radius and Reynolds number on variation of pitching-moment coefficient with angle of attack for body-wing-tail model.
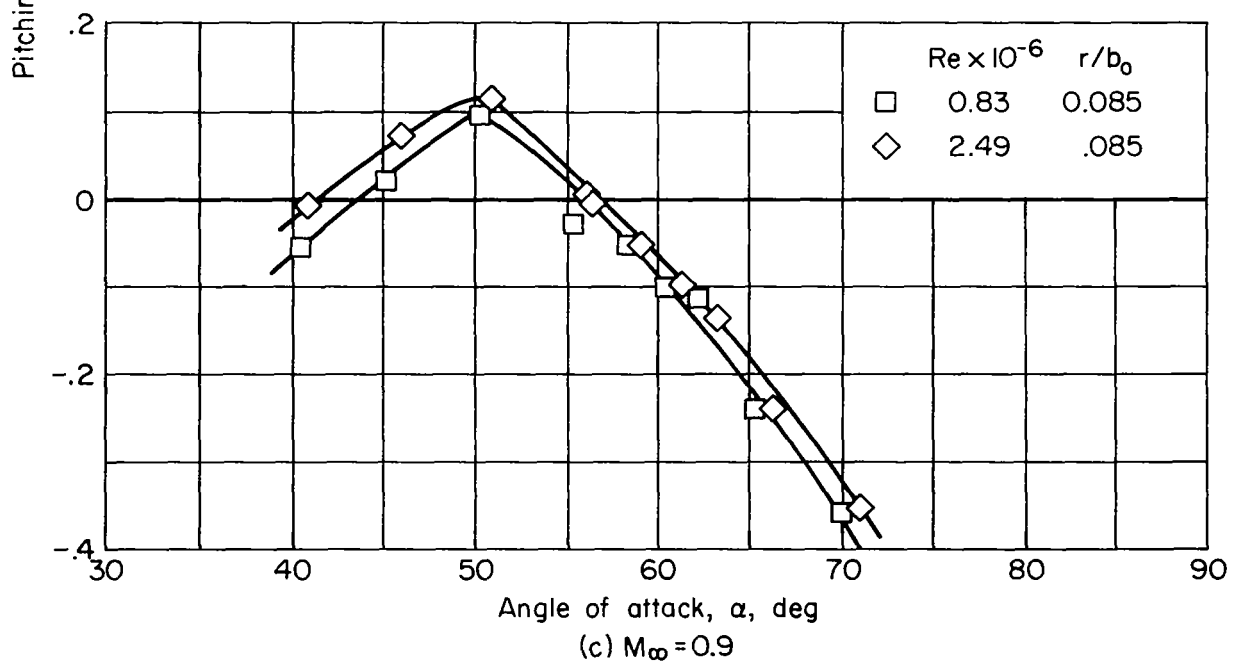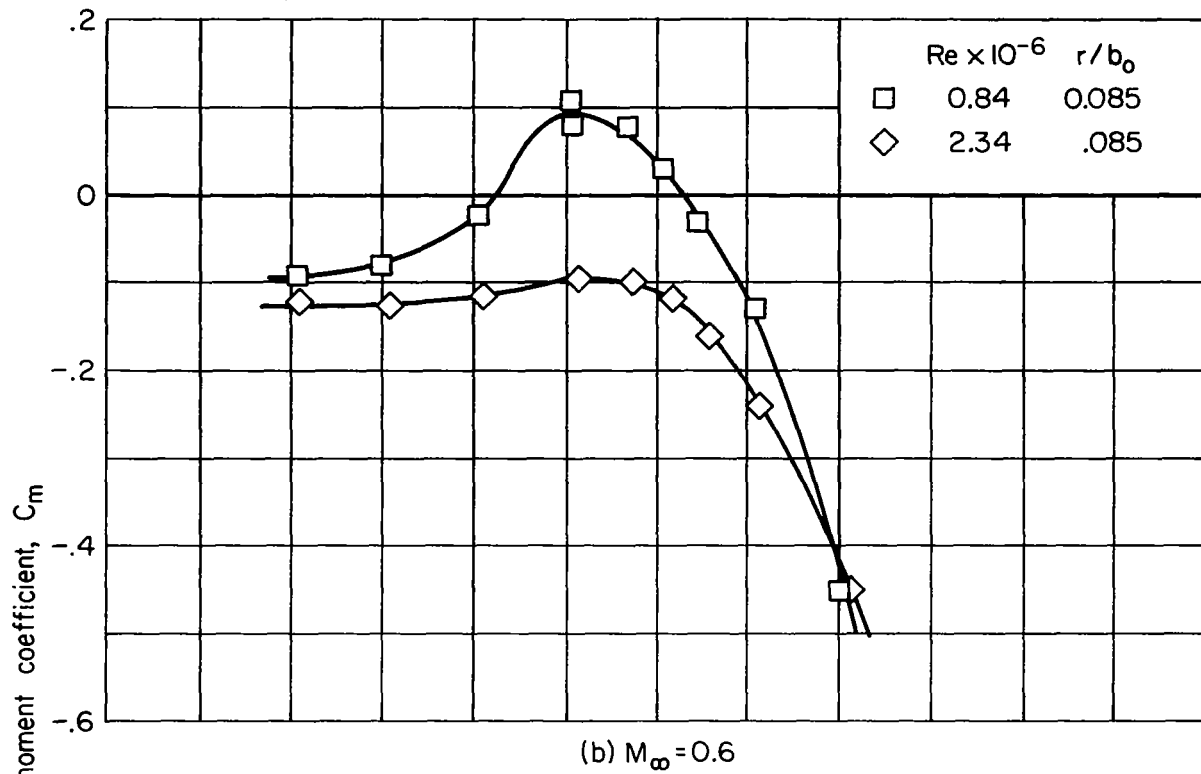
(b) $M_\infty = 0.6$
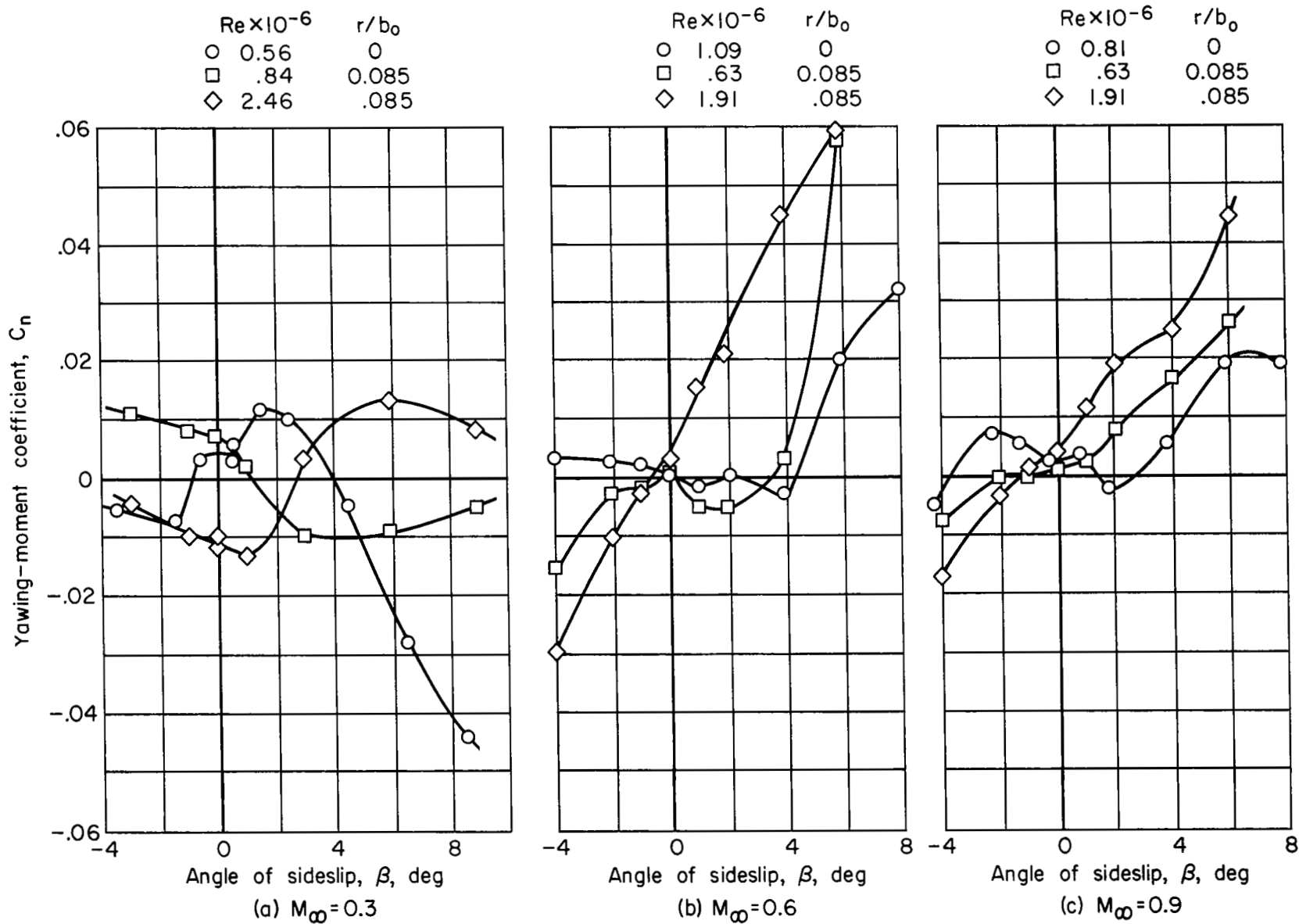
(c) $M_\infty = 0.9$

Figure 14.- Concluded.

Figure 15.- Effects of body corner radius and Reynolds number on variation of yawing-moment coefficient with angle of sideslip for body-wing-tail model at $\alpha \approx 60°$.